



Towards the retrieval of tropospheric ozone with the Ozone Monitoring Instrument (OMI)

T. Mielonen^{1,2}, J. F. de Haan¹, J. C. A. van Peet¹, M. Eremenko³, and J. P. Veefkind^{1,4}

¹Royal Netherlands Meteorological Institute (KNMI), De Bilt, the Netherlands

²Finnish Meteorological Institute, Kuopio, Finland

³Laboratoire Interuniversitaire des Systemes Atmospheriques (LISA), CNRS/Univ. Paris 12 et 7, Créteil, France

⁴Delft University of Technology, Delft, the Netherlands

Correspondence to: T. Mielonen (tero.mielonen@fmi.fi)

Received: 31 January 2014 – Published in Atmos. Meas. Tech. Discuss.: 25 February 2014

Revised: 13 January 2015 – Accepted: 16 January 2015 – Published: 9 February 2015

Abstract. We have assessed the sensitivity of the operational Ozone Monitoring Instrument (OMI) ozone profile retrieval algorithm to a number of a priori and radiative transfer assumptions. We studied the effect of stray light correction, surface albedo assumptions and a priori ozone profiles on the retrieved ozone profile. Then, we studied how to modify the algorithm to improve the retrieval of tropospheric ozone. We found that stray light corrections have a significant effect on the retrieved ozone profile but mainly at high altitudes. Surface albedo assumptions, on the other hand, have the largest impact at the lowest layers. Choice of an ozone profile climatology which is used as a priori information has small effects on the retrievals at all altitudes. However, the usage of climatological a priori covariance matrix has a significant effect. Based on these sensitivity tests, we made several modifications to the retrieval algorithm: the a priori ozone climatology was replaced with a new tropopause-dependent climatology, the a priori covariance matrix was calculated from the climatological ozone variability values, and the surface albedo was assumed to be linearly dependent on wavelength in the 311.5–330 nm channel. As expected, we found that the a priori covariance matrix basically defines the vertical distribution of degrees of freedom for a retrieval. Moreover, our case study over Europe showed that the modified version produced over 10 % smaller ozone abundances in the troposphere which reduced the systematic overestimation of ozone in the retrieval algorithm and improved correspondence with Infrared Atmospheric Sounding Instrument (IASI) retrievals. The comparison with ozonesonde measurements over North America showed that the operational retrieval performed

better in the upper troposphere/lower stratosphere (UTLS), whereas the modified version improved the retrievals in the lower troposphere and upper stratosphere. These comparisons showed that the systematic biases in the OMI ozone profile retrievals are not caused by the a priori information but by some still unidentified problem in the radiative transfer modelling. Instead, the a priori information pushes the systematically wrong ozone profiles towards the true values. The smaller weight of the a priori information in the modified retrieval leads to better visibility of tropospheric ozone structures, because it has a smaller tendency to damp the variability of the retrievals in the troposphere. In summary, the modified retrieval unmasks systematic problems in the radiative transfer/instrument model and is more sensitive to tropospheric ozone variation; that is, it is able to capture the tropospheric ozone morphology better.

1 Introduction

Atmospheric ozone occurs both in the stratosphere and the troposphere. In the stratosphere, ozone acts as a shield that protects the surface from energetic ultraviolet radiation. Tropospheric ozone, on the other hand, is a greenhouse gas that warms the atmosphere (Forster and Shine, 1997). Moreover, at ground level it is a pollutant and it causes respiratory problems in humans and damages crops. Tropospheric ozone is a short-lived species when compared with transport times (22 days in the troposphere), and therefore inhomogeneously mixed. A large fraction of the precursors of tropo-

spheric ozone are emitted from anthropogenic sources (Shindell et al., 2006). In order to understand the ozone-related physical and chemical processes in the atmosphere, global measurements of vertical ozone profiles are essential. Consequently, the total ozone column and ozone profiles have been monitored with spaceborne instruments since the late 1970s. Over the years, several methods have been developed for ozone monitoring: instruments use either limb or nadir viewing geometries and spectral regions range from ultraviolet to microwave. Limb emission and occultation instruments have good vertical resolution but their horizontal resolution is limited and they are not able to detect ozone in the lower troposphere. Microwave and thermal infrared (TIR) measurements can be done during night and day whereas ultraviolet measurements are limited to daytime. However, nadir UV and TIR measurements have much better horizontal resolution than the other methods. As part of this line of instruments the Ozone Monitoring Instrument (OMI; Levelt et al., 2006a, b) on-board Earth Observing System (EOS) Aura (Schoeberl et al., 2006) satellite was launched in 2004. Currently, two algorithms are used to retrieve ozone profiles from the OMI measurements: the operational OMO3PR retrieval developed at KNMI (Kroon et al., 2011) and a scientific algorithm developed at NASA (Liu et al., 2010). Both algorithms are based on the optimal estimation retrieval technique (Rodgers, 2000) but they differ in the implementation. For example, the algorithms use different radiometric calibration, radiative transfer models, vertical grids and a priori covariance matrices. The OMO3PR retrieval provides global coverage on daily basis with a vertical resolution of 6–7 km. Kroon et al. (2011) validated the retrieved ozone profiles with several satellite products and balloon-borne ozonesondes. As the summary in Table 1 shows, OMO3PR retrievals were in agreement with the Microwave Limb Sounder (MLS; Waters et al., 2006) retrievals within $\pm 10\%$ except for the Polar regions during the ozone hole seasons where differences up to $\pm 30\%$ were found. In addition, the comparisons with MLS and other correlative data sets showed that the biases vary with altitude. Furthermore, they found that OMI overestimates tropospheric ozone abundances from 0 to 30 %, when compared with MLS, the Tropospheric Emission Spectrometer (TES; Beer et al., 2001) and ozonesondes.

In this work, we studied how different assumptions in the OMO3PR retrieval affect the results and searched for possibilities to improve the accuracy of the retrieval in the troposphere. We concentrated on the a priori information: ozone climatology and the corresponding a priori covariance matrix, wavelength dependency of surface albedo, and stray light correction. In addition to a priori assumptions the retrieval is also affected by a number of other things, e.g. correction for rotational Raman scattering in the L1B reflectance data and cloud properties obtained from longer wavelengths. However, we limited this work to parameters that could be modified within the OMO3PR algorithm. First, we tested how sensitive the algorithm is to these a pri-

ori assumptions. Then, we implemented those a priori assumptions which appeared to improve the algorithm's performance in the troposphere. Finally, we evaluated the modifications done to the algorithm with two case studies. In the first case study, we compared the operational and the modified retrievals of tropospheric ozone over Europe to the results presented in the paper by Eremenko et al. (2008). In their work, Eremenko et al. (2008) used ozone profiles retrieved with an analytical altitude-dependent regularization method from the Infrared Atmospheric Sounding Interferometer (IASI; Clerbaux et al., 2009) data. IASI ozone profiles have been thoroughly validated for example by Keim et al. (2009) and Dufour et al. (2012). In the second case study, we compared the operational and modified ozone profiles against ozonesonde data from North America for August–September 2006. The ozonesonde data were downloaded from the World Ozone and Ultraviolet Radiation Data Center (WOUDC, www.woudc.org).

The main goal of this study is to examine if an UV instrument such as OMI could be used to retrieve tropospheric ozone abundance which has a significant effect on air quality.

2 OMO3PR algorithm

OMI is an instrument on-board the NASA Earth Observing System (EOS) Aura satellite. It is a nadir viewing, ultraviolet-visible (270–500 nm) imaging spectrometer, which provides daily global coverage with high spatial and spectral resolution (Levelt et al., 2006a, b). It has been measuring since 2004.

A detailed description of the operational OMI ozone profile algorithm (OMO3PR) is given by Kroon et al. (2011). Briefly, the retrieval exploits the information provided by the strong decrease in the ozone absorption cross-section between wavelengths of 270 and 330 nm. The radiation at the longer wavelengths traverses the whole atmosphere while the shortest wavelengths are only affected by the highest layers of the atmosphere. Therefore, spectral information of UV radiation can provide information on the vertical distribution of ozone. The measurements are taken from the UV1 channel (270.0–308.5 nm) and the first part of the UV2 channel (311.5–330.0 nm). The retrieval algorithm uses optimal estimation (Rodgers, 2000; termed maximum a posteriori method in the book), where the difference between the measured and modelled sun-normalized radiance is minimized iteratively by adjusting the amount of ozone in 18 atmospheric layers. This method requires a priori information on ozone profiles and other parameters like the surface albedo in order to constrain the retrievals. The OMO3PR retrieval uses the LLM ozone climatology (McPeters et al., 2007), which varies with month and latitude. The a priori ozone profiles are given constant relative variability of 20 % except for ozone hole conditions. Ozone hole conditions are assumed to occur between August and December at latitudes south of 50° S.

Table 1. The agreement between OMO3PR and other ozone profile observations in percent. Summarized from Kroon et al. (2011). The instruments used in the study are the Microwave Limb Sounder (MLS), the Tropospheric Emission Spectrometer (TES), the Stratospheric Aerosol and Gas Experiment (SAGE II; McCormick et al., 1989), the Halogen Occultation Experiment (HALOE; Russell III et al., 1993), the Optical Spectrograph and Infrared Imager System (OSIRIS; Llewellyn et al., 2004), the Global Ozone Monitoring by the Occultation of Stars (GOMOS; Bertaux et al., 2010) and balloon-borne ozonesondes (ECC).

	Tropical	Mid-latitude	Polar
OMI – MLS [%]	±10	±10	±30
OMI – TES [%]	±20	±30	±60
OMI – SAGE II [%]	10–60	20–40	
OMI – HALOE [%]	> 30	> 30	
OMI – OSIRIS/GOMOS [%]		±10	–15 to 20
OMI – ECC [%]	5–10 (< 30 hPa) up to 80 (30–200 hPa) 5–60 (> 200 hPa)	5–10 (20–50 hPa) up to 50–60 (> 50 hPa)	10–20

There, the variability is 60 % for altitudes between 21 and 50 km, and 30 % for the other altitudes. These settings are ad hoc assumptions and, therefore, not necessarily the best possible a priori knowledge in the sense of information theory. Thus it is worthwhile to test what can be achieved by changing these assumptions towards a climatologically valid a priori. The vertical correlation length of ozone is an a priori constraint and it is set to 6 km. To ensure that the retrieved ozone volume mixing ratios are positive, the algorithm operates with logarithm of the volume mixing ratio for each layer.

The surface albedo is also fitted in the retrieval and the OMI surface albedo climatology (Kleipool et al., 2008) is used as an initial value for the surface underneath the atmosphere. If the cloud fraction taken from the dedicated OMI cloud product (OMCLDO2; Acarreta et al., 2004) is lower than 0.2, surface albedos are fitted. Otherwise, cloud albedo values are fitted. The wavelength dependence of the albedo in both UV1 and UV2 channels is described with a second-order polynomial. Surface albedo is fitted for all wavelengths (although the shortest ones do not “see” the surface due to ozone absorption in the atmosphere) to partly account for the presence of aerosols which are not known or modelled specifically in the retrieval. Clouds are taken into account with a simple Lambertian cloud model. The vertical location (cloud pressure) and the effective cloud fraction are taken from the OMCLDO2 product and a fixed a priori albedo is used.

Stray light refers to light of other wavelengths that is scattered by the imperfect OMI optics onto the CCD detector and is registered at wrong wavelengths. This effect is more pronounced in the UV1 channel than in the UV2 channel because the detected radiances at the shorter wavelengths are smaller and, therefore, small amounts of radiance from other wavelengths can have a large effect on the measured signals. The shortest wavelengths are reflected only from the highest altitude layers in the atmosphere – thus, stray light has the largest effect on the retrieval of ozone at these altitudes. Hardly any stray light is expected at longer wavelengths but

it can be several percent at short wavelengths, depending in part on the amount of clouds in the pixel considered. Roughly 10 % stray light at 270 nm corresponds to 1 % stray light at 300 nm and 0.03 % or less at 330 nm, assuming wavelength-independent additive stray light. This is due to the design of the OMI instrument. For the tropospheric ozone retrieval the main source of information is the wavelength range 320–330 nm – thus, stray light does not affect the retrieval significantly. Dobber et al. (2006) have provided a detailed description of stray light features in the OMI instrument. Regarding the ozone profile retrieval, correction for stray light is done in two steps. The first correction is done during the production of the LIB spectra (OMLIBRUG; van der Oord et al., 2006). In this correction, specific wavelength ranges are used to define so-called source and target regions. For the source regions averaged signals are calculated using the information over the whole swath. Then, these signals are multiplied by a polynomial that distributes the stray light over the target regions. Finally, the signals are subtracted from all the pixels in the corresponding target areas. The second stray light correction is part of the optimal estimation in the OMO3PR algorithm. There, stray light is described with second-order polynomials for both UV channels separately.

The surface is modelled using a Lambertian reflector: bi-directional reflectance properties are ignored. In view of the large amount of Rayleigh scattering in the atmosphere at UV wavelengths, specific bi-directional surface reflectance properties cannot be observed above the atmosphere (scattering washes the bi-directional properties out). Only the average reflectance properties (averaged over the bidirectional properties) affect the light arriving at the sensor. Therefore, we expect that a Lambertian surface is a good model for the surface reflectance. Furthermore, we can distinguish between instrumental stray light which contains no spectral features due to ozone absorption and radiance that has been reflected by the surface which does contain spectral features due to ozone absorption. This makes it possible to fit stray light and surface albedo separately.

Table 2. Content of the optimal estimation state vector and the related a priori information used in the OMO3PR retrieval.

Optimal estimation state vector		a priori information	a priori variability
Species	Number of elements		
O3 profile	18	LLM climatology (McPeters et al., 2007)	20 % (For ozone-hole conditions 60 % (21–50 km) and 30 % for other altitudes)
Surface albedo (surface or cloud)	6	OMI surface albedo climatology (Kleipool et al., 2008), 0.8 for clouds	100 %
Stray light	6	0	100 %

Table 2 summarizes the above-mentioned information. It presents the content of the optimal estimation state vector used in the OMO3PR retrieval. The state vector contains the ozone profile represented with 18 layers and six values for both surface albedo and stray light. In the operational retrieval, the effect of NO₂, SO₂ and aerosols are not considered. In addition to the actual ozone product, the OMO3PR algorithm produces diagnostic quantities, like posterior error and averaging kernel, that can be used to evaluate the retrieval. Table 3 presents the layers and the corresponding pressures used in the retrieval.

3 Sensitivity studies

3.1 Stray light

To study the sensitivity of the retrieval to the stray light corrections we turned off the two corrections separately and at the same time and processed an orbit (18 October 2005, orbit 06704, 1496 × 30 pixels) with all these different setups of the algorithm. Then, we studied how the retrieved ozone profiles changed on average and in six different latitude bands. Regarding the aim of this work, we concentrated on the effects in the troposphere. Figure 1 presents the difference between the operational and modified ozone profile retrievals for the whole orbit. The error bars in the plot represent the standard deviation of the difference for each layer. Figure 1a shows that the differences between the operational retrieval and the retrieval without stray light corrections are large and oscillating, 10–20 % on average. Moreover, the number of converged retrievals dropped dramatically, from 40 000 to about 13 000 in the studied orbit (06704). This confirms that stray light correction is essential for the convergence of the algorithm. The ozone changes implied by the different stray light schemes seem to reduce the discrepancies between the operational OMI retrieval and MLS results as presented by Kroon et al. (2011) in some but not all latitude bands. Even though the signs of the changes in the ozone amounts seem to reduce oscillation in the difference between the instruments at some latitude bands, the retrieval without stray light correc-

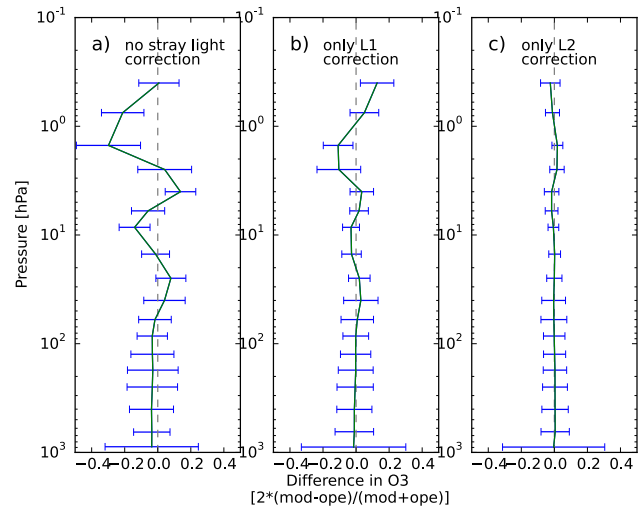


Figure 1. Effect of stray light corrections. Change in the ozone profiles when the retrieval has no stray light correction (a), only L1 correction (b), and only L2 correction (c), compared to the operational algorithm which includes both types of correction. Error bars show the standard deviation of the difference; mod and ope refer to the modified and operational versions of the algorithm, respectively.

tion could change the results too much and turn underestimated retrievals into overestimated and vice versa.

Turning off the Level 1 (L1) stray light correction while doing the Level 2 (L2) correction caused only minor changes in the ozone profiles, as can be seen from Fig. 1c. As the plot shows, the systematic changes are small at higher altitudes and almost nonexistent in the troposphere. Moreover, the usage of the L2 stray light correction reduces the variability at all altitudes as can be seen by comparing the error bars from plot 1c with 1a and 1b. The large variations at the lowest altitudes are caused by cloud-free retrievals (cloud fraction < 0.1) where the retrievals without complete stray light correction produce over 10 times larger ozone amounts than the operational retrieval.

Turning off the L2 stray light correction affected the ozone profiles mainly in the stratosphere, as Fig. 1b shows. For

Table 3. Pressure levels of the layer edges for the operational (ope) and for the modified (mod) pressure grids in hectopascals (hPa).

	0	1	2	3	4	5	6	7	8	9	10	11	12	13	14	15	16	17	18
ope	0.3	0.5	1.0	2.0	3.0	5.0	7.0	10	20	30	50	70	100	150	200	300	500	700	1000
mod	0.2	0.32	0.52	0.83	1.3	2.1	3.4	5.5	8.8	14	23	36	58	94	150	240	390	620	1000

some layers, the changes can be up to 20% but on average they stay below 10%. In the troposphere, the average difference is well below 10%. When comparing these values with the validation results shown in Table 1, it is evident that the effect of stray light correction is too small to explain completely the systematic differences between the OMI and other ozone profile retrievals. Moreover, the retrieval of tropospheric ozone profiles is not that sensitive to stray light, thus, its correction is accurate enough for these layers.

3.2 Surface albedo parameterization

As mentioned in Sect. 2, the operational version of the retrieval algorithm uses second-order polynomials to describe the dependency of surface albedo on wavelength at both UV1 and UV2 channels separately. To study the sensitivity of the retrieval to this assumption we varied the wavelength dependencies of the albedos. We tested constant, first-order (linear) and second-order polynomials for both channels separately. We processed all the pixels from one orbit (06704, 1496×30 pixels) and studied how the ozone profiles change when compared to the operational product on average and in six different latitude bands. In the comparison, we concentrated on tropospheric features. To our knowledge, there is no applicable surface albedo database for these wavelengths which could be used to select the most physical representation for the wavelength dependency. Therefore, we decided to concentrate on the configuration that provided the largest decrease in the tropospheric ozone: we wanted to test the hypothesis that the known high bias of OMI tropospheric ozone could be a consequence of an inappropriate parameterization of surface albedo. Kroon et al. (2011) had shown that OMI ozone values were consistently larger than TES or ozonesonde values in the troposphere, and the amount of overestimation varied from a few percent to at least 30% depending on the latitude band.

Figure 2 presents comparisons of two modified albedo parameterizations against the operational retrieval for the whole orbit. Other parameterizations were also tested but we show here only the most suitable ones. The largest decrease in tropospheric ozone was found by using a second-order polynomial at UV1 channel and a constant value at UV2 channel (Fig. 2b). The largest decrease in ozone levels were found (over 20% on average) in the Arctic and in the southern mid latitudes but the changes were small near the equator (see Supplement Fig. S1b). If a first-order polynomial (linear fit) was used for the surface albedo at both channels, the amount

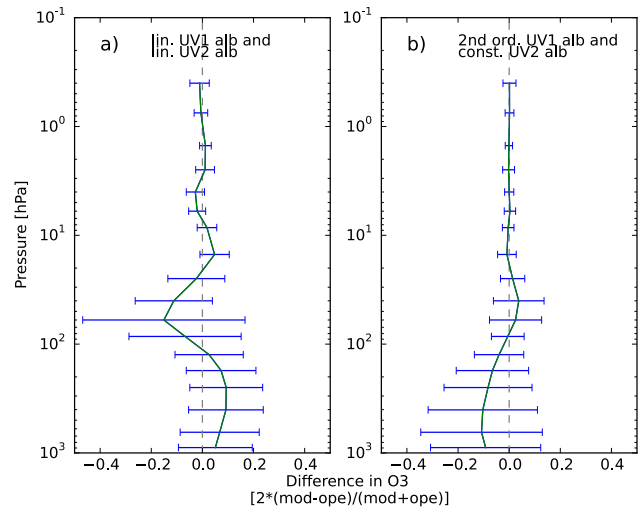


Figure 2. Effect of albedo assumptions: (a) assuming linear albedos at both UV1 and UV2 channels instead of second-order polynomials; (b) assuming constant albedo at UV2 channel instead of second-order polynomial. Error bars show the standard deviation of the difference; mod and ope refer to the modified and operational versions of the algorithm, respectively.

of tropospheric ozone increased up to 10% on average, as Fig. 2a shows. However, this modification can also decrease ozone amounts at some latitudes but mainly it increases them as the averaged profile implies (see Fig. S1a). Therefore, this setup was not considered usable for our purposes.

3.3 A priori information

To constrain the retrievals, the OMO3PR algorithm uses climatological ozone profiles (LLM; McPeters et al., 2007) as a priori information. In addition to the profiles themselves, a priori information on the variability of ozone at each layer is used. Recently, two new ozone climatologies became available: McPeters and Labow (2012) (henceforth ML), and Sofieva et al. (2014) (henceforth TpO3).

The ML climatology is formed by combining ozone soundings and MLS data. The climatology consists of monthly average ozone profiles and standard deviation for 10° latitude zones with altitudes from 0 to 66 km. A more detailed description of the climatology is given by McPeters and Labow (2012).

The TpO3 climatology is based on a combination of ozone soundings and SAGE II (McCormick et al., 1989) satellite

data. Mean ozone profiles and standard deviations are given for 10° latitude zones and for each month. The ozone mixing ratio profiles are presented on a 1 km vertical grid. In addition, the profiles are grouped for tropopause heights in 1 km intervals. This is an important addition because variation in the tropopause height is the main driver for the variability in climatological ozone values in the upper troposphere and lower stratosphere (Sofieva et al., 2014). This variability increases the a priori variability in this altitude range. The tropopause heights have values between 6 and 17 km but the number and altitude of the tropopause heights vary for different latitude bands and months. In order to have constant dimensions for the a priori ozone look-up table in the OMO3PR algorithm, all latitude and month cases were assigned to 12 tropopause heights. The tropopause height was calculated in the retrieval algorithm using temperature profiles from ECMWF data following the guidelines given by Sofieva et al. (2014). If a calculated tropopause height was outside the range of the climatological tropopause heights, the nearest climatological value was assigned for it or an average of the two closest ones was used.

In order to test how the usage of these climatologies affect the ozone retrievals, we processed two orbits (18 October 2005, orbits 06702 and 06704) using all three climatologies. For the evaluation, every 10th measurement and 10 pixels for each measurement from the middle of the swath were taken into account. In the comparisons we used the new climatologies with the operational a priori covariance matrix (20 % variability, except for ozone hole conditions) and with a priori covariance matrices calculated from the variability values given in the climatologies. Here the diagonal values on the retrieval grid were obtained using interpolation. Next, a correlation length of 6 km was used to calculate the nondiagonal elements of the a priori covariance matrix.

3.3.1 ML climatology

In the first comparison, we only changed the average ozone profiles and used the operational a priori covariance matrix. This combination produced the largest differences at the highest altitudes when compared with the operational retrieval (Fig. 3a). This was expected because when compared with the operational (LLM) climatology the largest changes between the climatologies are at the top of the profiles. In addition, the amount of ozone increases around 200 hPa.

In the second comparison, we replaced the operational a priori covariance matrix with a climatological one that was calculated from the variability values given in the climatology. For this case, as Fig. 3c shows, the highest altitudes do not change much. For most of the studied latitude bands the amount of tropospheric ozone is decreased close to the surface but increased higher up (see Fig. S2). At altitudes below 10 hPa the difference with the operational retrieval shows an oscillating behaviour that increases towards lower altitudes. This is caused by the larger a priori variability of ozone in

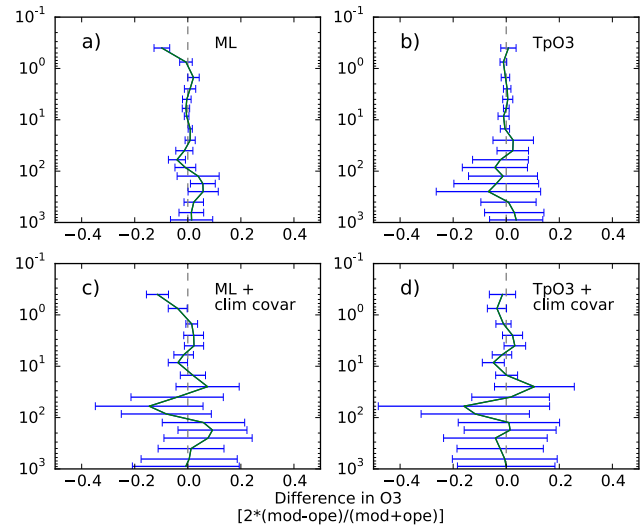


Figure 3. Change in ozone profiles when ML (a) and TropO3 (b) are used with the operational a priori covariance matrices. Change in ozone profiles when ML (c) and TropO3 (d) are used with climatological covariance matrices. Error bars show the standard deviation of the difference; mod and ope refer to the modified and operational versions of the algorithm, respectively.

the troposphere as can be seen from Fig. 4, which presents the a priori variability and posterior errors for the retrievals with different ozone climatologies. In the stratosphere the ML a priori variability (Fig. 4, green dashed line) is much smaller than the operational values but for pressure levels above 50 hPa the situation is the opposite. For the posterior errors (solid green line) the situation is similar. This can also be seen from Table 4 which presents the mean a priori variability and posterior errors for the different retrieval versions. The unweighted mean variabilities and errors are calculated for the whole profile and for the lower part of the atmosphere in order to highlight the change at the lowest altitudes. Regarding the values for the whole profile, the ML variabilities and errors are close to the operational ones. However, at the lowest altitudes ML values are significantly larger (a priori $\sim 60\%$ larger, posterior $\sim 35\%$ larger).

3.3.2 TpO3 climatology

For the first comparison with the TpO3 climatology, we used the operational a priori covariance matrix in both retrievals. As Fig. 3b shows, the largest differences are seen around 200 hPa, TropO3 giving smaller ozone values than the operational retrieval.

When the operational a priori covariance matrix was replaced with a climatological version, the differences in the retrieved ozone profiles grew larger, as Fig. 3d shows. The differences around 50 hPa are larger and the profile oscillates more. Furthermore, for most of the studied latitude bands the amount of tropospheric ozone is decreased, except for the

Table 4. Mean a priori variability and posterior errors in percent for three retrievals: operational, with ML ozone climatology and with TpO3 climatology. Mean unweighted variabilities and errors are presented for the whole profile and for lower atmosphere (> 100 hPa). The values are calculated from the data presented in Fig. 4.

a priori	Operational	ML	TpO3
Whole column	19.8 %	20.6 %	16.6 %
Lower atmosphere (> 100 hPa)	19.5 %	30.7 %	28.8 %
posterior			
Whole column	10.5 %	12.0 %	10.0 %
Lower atmosphere (> 100 hPa)	15.5 %	21.0 %	19.2 %

lowest layers, where half of the latitude bands show an increase in ozone abundance (see Fig. S2b).

When comparing the results from the new climatologies with the operational one, it is important to notice that the new climatologies increase the amount of ozone in the troposphere on average, except when TpO3 is used with a climatological a priori covariance matrix.

Regarding the variability in the stratosphere, the TpO3 a priori variability (Fig. 4, red dashed line) is much smaller than the operational values but for altitudes below 60 hPa the situation is the opposite. For posterior errors (solid red line) the situation is similar. As Table 4 shows, the variabilities and errors of TpO3 for the whole column are slightly smaller than the operational ones – however, at the lowest altitudes TpO3 values are significantly larger (a priori $\sim 50\%$ larger, posterior $\sim 25\%$ larger). Both climatologies (TpO3 and ML) cause similar peaks in the difference plots between 10–100 hPa when climatological a priori covariances are used (Fig. 3c, d). This is caused by the similar uncertainty values in both climatologies for these altitudes. When compared with the ML variability, TpO3 variability is always smaller, except near the surface.

Visual comparison of difference profiles at different latitude bands with the OMI-MLS validation results presented by Kroon et al. (2011) indicates that the oscillating effects caused by the use of a climatological a priori covariance matrix might improve the agreement between MLS and OMI ozone profiles.

Based on these results, TpO3 appears as the most promising climatology for the improvement of tropospheric ozone retrievals. From the viewpoint of information theory it is justified to have a stronger constraint on stratospheric ozone and to allow more variation in tropospheric ozone because this corresponds better to our knowledge on ozone variability. As a next step, we tested how the albedo parameterizations combined with the TpO3 climatology (with operational a priori covariance matrix) affected the retrieved profiles. Figure 5 shows three comparisons with the operational retrieval: modified version with linear albedos at both channels (5a), con-

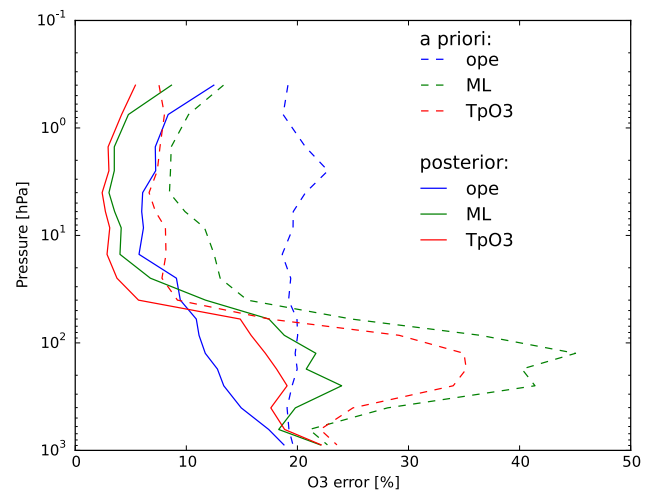


Figure 4. A priori variability (dashed lines) and posterior errors (solid lines) when different ozone climatologies are used. Operational retrieval is shown in blue, ML climatology in green and TpO3 climatology in red. The a priori variabilities for ML and TpO3 climatologies are based on the ozone variability reported in the respective climatologies.

stant albedo at UV2 channel (5b), or linear albedo at UV2 (5c). When compared with the results presented in Fig. 2, the effect of albedo parameterizations changed slightly. With the operational climatology the largest decrease in tropospheric ozone was achieved by using a constant albedo in the UV2 channel, whereas with the TpO3 climatology the largest decrease was achieved with a linear albedo in the UV2 albedo, as can be seen from Fig. 5.

3.4 Effect of modifications on averaging kernels and errors

In addition to the retrieved ozone profiles, the OMO3PR algorithm produces several diagnostic quantities that can be used to assess the retrievals. The averaging kernel is one of them. We compared averaging kernels from the different versions of the algorithm to study how the information content was distributed in the retrieved profiles. The degrees of freedom for a retrieval can be calculated as a sum of the diagonal elements of the averaging kernel. For this comparison, we calculated mean averaging kernels from 34 pixels from a region with high tropospheric ozone values (45–55° N, 20–30° E) on 17 July 2007, in order to have sufficient signal also from the lowest altitudes. Figure 6a shows the mean averaging kernel for the operational retrieval. From this plot it is evident that the operational retrieval has very little information from the troposphere. When the a priori ozone profiles are taken from the TpO3 climatology, the averaging kernel is almost identical with the operational one, as Fig. 6b shows. Moreover, the usage of linear albedo in the UV2 channel (with TpO3 climatology) does not have an effect on the aver-

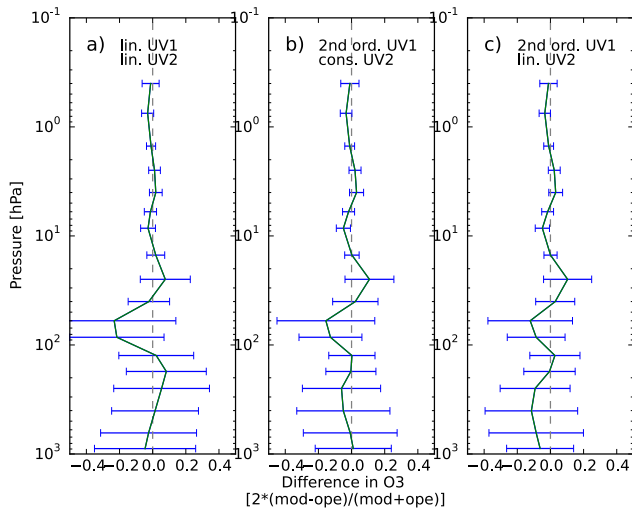


Figure 5. Effect of albedo assumptions with the TropO3 climatology: (a) assuming linear albedos at both UV1 and UV2 channels instead of second-order polynomials; (b) assuming constant albedo at UV2 channel; (c) assuming linear albedo at UV2 channel. Error bars show the standard deviation of the difference; mod and ope refer to the modified and operational versions of the algorithm, respectively.

aging kernels (Fig. 6c). When the operational a priori covariance matrix is replaced by a climatological version (based on the variability values from the TpO3 climatology) the averaging kernels change significantly (Fig. 6d). The information content increases in the troposphere and decreases at the highest levels. This is caused by the larger a priori variability values in the troposphere when compared with the operational retrieval which assumes 20 % variability there (see Fig. 4). The opposite holds true for the stratosphere. When a minimum value of 20 % is set to the variability in the climatological a priori covariance matrix, the averaging kernels change slightly (Fig. 6e). The degrees of freedom in the troposphere decrease while the degrees of freedom in the stratosphere increase. Figure 6f is the same as Fig. 6e but with a minimum variability of 10 %. By comparing these two plots, it is clear that smaller a priori variability values in the stratosphere produce more degrees of freedom in the troposphere and less in the stratosphere. As a whole, Fig. 6 shows that the distribution of degrees of freedom for a retrieval depend mainly on the selection of the variability values used in the a priori covariance matrix.

Above we discussed the effect of changes in the a priori covariance matrix on the degrees of freedom of the troposphere and stratosphere. Alternatively, one could discuss these changes in terms of changes in the vertical resolution of the retrieved profile, which provides essentially the same results. If the degrees of freedom of the troposphere increase, the vertical resolution in the troposphere will also increase.

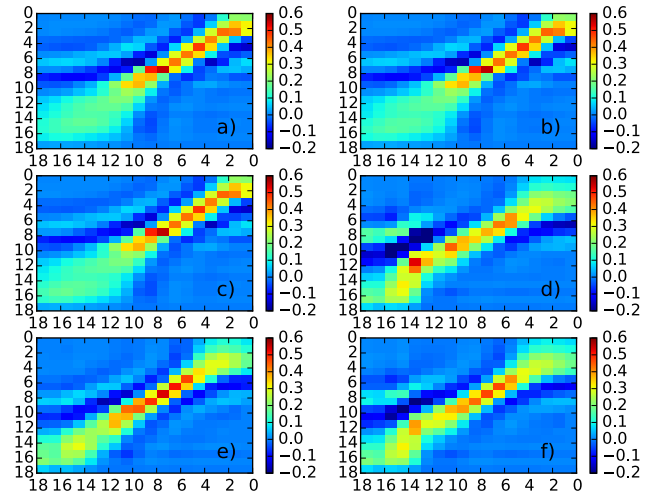


Figure 6. Mean averaging kernels from 34 pixels on the 17 July 2007 (45–55° N, 20–30° E) for the operational retrieval (a), with the TpO3 climatology (b), with TpO3 and linear albedo in UV2 channel (c), with TpO3, linear albedo in the UV2 channel and a climatological a priori covariance matrix (d), with a climatological a priori covariance matrix and minimum of 20 % variability (e) and with a climatological a priori covariance matrix and minimum of 10 % variability (TpO3_alb_covar_10) (f). Axis are the layer indices, 18 being the layer closest to the surface (the corresponding pressure levels are shown in Table 3).

Similarly, if the degrees of freedom of the troposphere decrease, the vertical resolution will also decrease.

In addition to the degrees of freedom, it is interesting to consider how these different a priori assumptions affect the a priori variability and posterior errors. Figure 7 presents the variabilities and errors for the discussed versions of the retrieval (dashed lines for a priori variability and solid lines for posterior errors). Figure 7a shows the variabilities and errors for the operational retrieval and for two versions with TpO3 climatology. The first version (TpO3) has the same albedo assumptions as the operational retrieval while for the second one (TpO3_alb) a linear albedo is assumed in the UV2 channel. As the dashed lines show, all the retrievals have the same a priori variabilities. The usage of the TpO3 climatology produces slightly smaller posterior errors than the operational version at some altitudes and the modified albedo only has a minor effect at the lowest altitude. Figure 7b shows the variabilities and errors for the retrieval versions with the TpO3 climatology, modified albedo and climatological a priori covariance matrix. For the first version (TpO3_alb_covar), the a priori variabilities are taken directly from the climatological variability values, thus they are small in the stratosphere. For the two other versions, minimum a priori variabilities were assumed to be either 10 % (TpO3_alb_covar_10) or 20 % (TpO3_alb_covar_20). The minimum a priori variability of 20 % was used in this analysis because it is also used in the operational retrieval, whereas the 10 % variability rep-

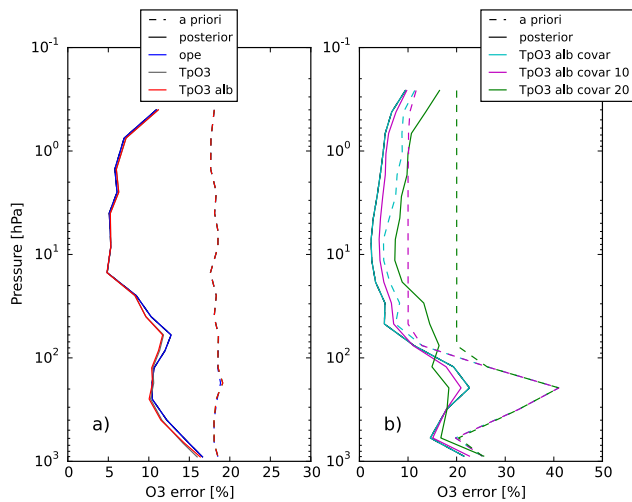


Figure 7. A priori variability (dashed lines) and posterior errors (solid lines) when different a priori covariance matrix assumptions are used. Operational retrieval is shown in blue, TpO3 climatology in green, TpO3 with linear UV2 albedo in red (a), TpO3 with climatological a priori variability in cyan, TpO3 with climatological a priori variability with minimum of 20% in black and TpO3 with climatological a priori variability with minimum of 10% in magenta (b).

resents the average variability in the stratosphere calculated from the ML and TpO3 climatologies. Constant relative variability values are used in the algorithm to avoid propagating unphysical structures arising from the climatological uncertainties. As the plot shows, posterior errors are significantly different for these versions. In the troposphere, the posterior errors are larger than for the retrievals with the operational a priori variability. In the stratosphere, smaller a priori variabilities produce smaller posterior errors which is to be expected. Although the errors look significantly different for the retrievals with operational and climatological a priori covariance matrices, the relative change between the a priori variability and posterior errors stay in the same range for all the versions, especially in the troposphere. In the stratosphere, the operational a priori covariance matrix produces slightly larger reduction in the uncertainty. Based on these results it seems that all the retrieval versions are as effective in reducing the uncertainty and that the posterior error values depend mostly on the assumed a priori variability. This means that posterior errors are not a useful metric for comparing the performance of different retrieval algorithms.

We also studied how the quality of the fit was affected by the different versions of the algorithm by comparing the root mean square errors of the fits (RMSE). For this, we used a data set over Europe (see Sect. 4.1 for more details). In principle, any modification that improves the fit in the Huggins band (320–360 nm) could be expected to improve the tropospheric ozone retrieval, since this part of the measurement contains the available information on tropospheric ozone. As

the sun-normalized radiance is much larger at longer wavelengths the RMSE is representative for the fit in the Huggins band. The differences between averaged RMSE values for different retrievals were only about 0.01 % smaller on average – thus, basically the modification of the a priori assumptions does not affect the quality of the fit.

Based on the sensitivity tests discussed in this section and our aim to improve the accuracy of the OMO3PR retrievals in the troposphere, we decided to make the following modifications to the algorithm: (1) we replaced the LLM ozone climatology with the TpO3 climatology, (2) we replaced the operational a priori covariance matrix with a climatological version that is based on the variability from the TpO3 climatology (with min. 10 % standard deviation, separated tropo- and stratosphere), and (3) we replaced the second-order polynomial for the albedo in the UV2 channel with a first-order polynomial. We use a block diagonal matrix with no covariances between the tropospheric and the stratospheric blocks, although, our sensitivity studies (not shown) did not show visible effects in ozone abundances caused by this modification. In addition, we updated the retrieval’s vertical pressure grid to $P_i = 2^{-i \cdot 1.37/2} \cdot 1000$ for $i = 0, 18$ which follows the principles presented by Liu et al. (2010) without changing the number of layers (see Table 3). We also tested how sensitive the retrieval is to the selection of the correlation length. The operational retrieval uses correlation length of 6 km – thus, we tested how the retrieved ozone abundances change if correlation lengths of 1, 3 or 12 km are used instead. Our comparisons showed that the dependence of the result on the chosen correlation length was generally small except for a correlation length of 1 km which led to excessive oscillations in the retrieved profiles. Based on these results we decided to use the correlation length used in the operational retrieval also in the modified algorithm. The correlation length was used for both the stratospheric and tropospheric blocks of the covariance matrix.

4 Evaluation of the modified algorithm

To evaluate the usefulness of our modifications and as a step towards validation of the modified retrieval setup, our tropospheric ozone retrievals were compared to two sets of independent measurements. In the first validation study, we compared our retrievals with the IASI results published by Eremlenko et al. (2008), and in the second study we compared the retrievals with ozonesondes over North America.

4.1 Case study Europe

The modified version of the algorithm uses a different pressure grid than the operational one, thus we had to interpolate the profiles in order to compare values for the exactly same altitude range. This was done by calculating a cumulative ozone profile in Dobson units from the sur-

face to the top of the atmosphere. The cumulative profile at altitude z is the integral of the ozone density from surface to altitude z , transformed into Dobson units. Then, the cumulative profile could be interpolated without changing the total ozone amount in the column. Finally, the tropospheric ozone abundance was taken from the 400 hPa level which corresponds to the altitude of 6 km used in the analysis by Eremenko et al. (2008). For the comparison, we calculated the ozone profiles first in Dobson units from the cumulative profile and then transferred the layer values into mixing ratios with the following equation: $\text{vmr} = \text{dobs} / (\text{pres}_{\text{bottom}} - \text{pres}_{\text{top}}) \cdot 1.26720 \times 10^{-6}$, where dobs is the ozone abundance of a layer in Dobson units, $\text{pres}_{\text{bottom}}$ is the pressure at the bottom of the layer, and pres_{top} is the pressure at the top of the layer. The constant is required to transfer the Dobson units into volume mixing ratios.

Eremenko et al. (2008) compared tropospheric ozone columns from IASI retrievals with predicted values from the CHIMERE model for 3 days in July 2007. We processed the same dates with different versions of the OMO3PR algorithm (using every second measurement and retrievals with cloud fraction < 0.3) to study how modifications in the algorithm affected the retrieved tropospheric ozone abundances. Here, we concentrate on results from a single day, 17 July 2007, because during this day high tropospheric ozone values occurred in eastern Europe (48–56° N, 20–30° E; see Fig. S3c). Before comparing the modified OMO3PR retrievals with the IASI results, we studied how the modifications of the algorithm affected the spatial distribution of tropospheric ozone for this day. For the total ozone columns the changes were smaller than 0.1%. Figure 8 shows the difference between the operational retrieval and the modified versions in percent. The averaged values for the studied region are given in Table 4. The usage of the TpO3 climatology (Fig. 8a) decreases the amount of tropospheric ozone at Bay of Biscay (42–48° N, 10° W–0° E) and increases it in eastern Europe (42–60° N, 20–30° E). However, on average the change is only 0.6%. The usage of a linear albedo at the UV2 channel does not have as large an effect as the climatology on the spatial distribution of ozone (Fig. 8b). However, decrease in ozone abundance can be seen in northern Europe (above 54° N) and on average, the decrease is 4.7%. The changes are mainly connected to cloud cover (see Fig. S4). When cloud cover (Fig. S4) is compared with the tropospheric ozone differences (Fig. 8b) it is clear that the modified albedo has the largest effect on partly cloudy pixels. The usage of a climatological a priori covariance matrix with a minimum variability of 10% (Fig. 11c) decreased the retrieved amount of tropospheric ozone everywhere (11.3% on average). These results highlight the fact that changes in the tropospheric ozone abundances caused by one modification can be cancelled out by another modification. The squared structures in Fig. 8 originate from the calculated tropopause heights. The heights are calculated with 1 km vertical resolution from

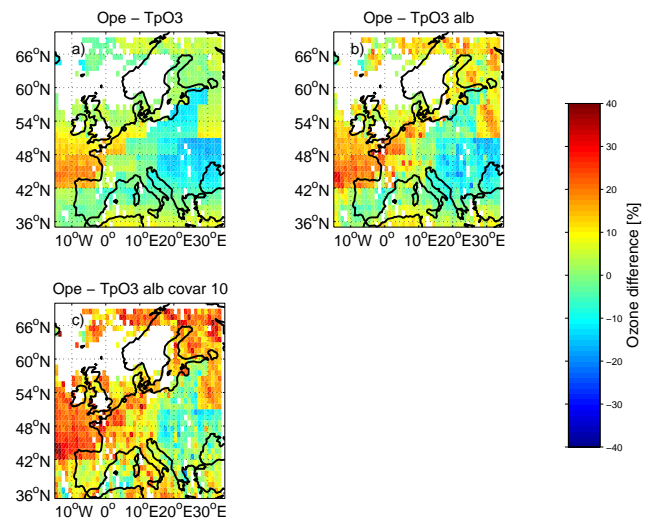


Figure 8. Difference in tropospheric ozone abundances (up to 400 hPa) between operational (ope) and modified OMO3PR retrievals on 17 July 2007. Modified versions of the OMI retrieval algorithm are: TropO3 climatology and operational albedo (a), TropO3 climatology and linear albedo in UV2 (b), and TropO3 climatology, linear albedo in UV2 and climatological a priori covariance matrix (c). Daily data averaged on 1×1 grid. Averaged differences are given in Table 4.

ECMWF data which have a spatial resolution of $1 \times 1^\circ$. The coarse vertical resolution combined with the spatial resolution of the ECMWF data causes large areas to have the same tropopause height and the transition from one a priori profile to another can cause artificial structures that are visible in the difference plots. To check how dependent the retrieved tropospheric ozone abundances are on the selection of the tropopause height we studied the averaged tropospheric ozone values as a function of tropopause height from the operational, modified (Trop_alb_covar_10) and IASI retrievals (not shown). The variability of ozone within 1 km height bins was large while the differences between the heights were smaller. This indicates that the selection of the tropopause height does not constrain the retrieval of tropospheric ozone too much and that it does not mask the natural variability of tropospheric ozone.

As a next step, we compared all the OMI retrieval versions to the IASI retrieval for the same day, as presented in Fig. 9 and in Table 5. First, we did the comparison with the operational retrieval (Fig. 9a). The operational version overestimates the amount of ozone in western (42–54° N, 10° W–10° E) and northern (54–66° N, 20–30° E) parts of Europe and slightly underestimates in eastern Europe (48–56° N, 20–30° E) where IASI detected the high values. The usage of the TpO3 climatology (Fig. 9b) improves the correspondence in western Europe while changing the small underestimation in eastern Europe into a slight overestimation, thus, the new climatology did not improve the agreement for the highest

Table 5. Differences in tropospheric (up to 400 hPa \sim 6 km) ozone abundances between IASI and OMI retrievals for 17 July 2007 in Europe. Four different versions of the algorithm are used: Operational is the operational version, TpO3 refers to a version that uses the TpO3 climatology, TpO3_alb refers to a version that uses the TpO3 climatology and linear albedo in the UV2 channel, and TpO3_alb_covar_10 refers to a version that uses the TpO3 climatology, linear albedo in the UV2 channel and a climatological a priori covariance matrix. Average difference in Dobson units (Ave diff), average relative difference (Ave rel diff) and average standard deviation (Ave SD) are presented. In addition, the difference between the operational OMI retrieval and the other versions (Ave rel diff with ope) in percent are given.

17 July 2007	Operational	TpO3	TpO3_alb	TpO3_alb_covar_10
Ave diff [DU]	-5.06	-5.19	-4.32	-2.72
Ave rel diff	-0.23	-0.23	-0.19	-0.12
Ave SD	4.50	3.57	3.59	3.79
Ave rel diff with ope [%]		0.6	4.7	11.3

ozone values in eastern Europe. Then, we changed the albedo assumptions so that a linear albedo, instead of a second-order polynomial, was used in the UV2 channel (Fig. 9c). Based on the plot, this modification does not clearly improve the agreement, although the averaged values in Table 5 indicate some improvement (from overestimation of 23 to 19%). As a last step, we replaced the a priori covariance matrix with the climatological version (Fig. 9d). The usage of the new a priori covariance matrix clearly improves the agreement with IASI all over Europe (overestimation down to 12%) except for the highest ozone values in eastern Europe. This implies that the better correspondence with IASI was achieved by decreasing ozone abundances in regions with low ozone values and that the OMO3PR retrieval is not able to capture the high ozone values quite as well as IASI even after a number of modifications.

We also compared the absolute tropospheric ozone abundances from two versions of the OMO3PR algorithm with IASI (see Fig. S3). The operational version does not match the IASI results at all, whereas the modified version (Trop_alb_covar_10) is able to capture the ozone plume in eastern Europe (48–56° N, 20–30° E) better. Nevertheless, as Fig. 9d showed, the differences are still quite large there. One reason for this is probably the time difference between the measurements. The IASI measurements are taken around 09:30 local time whereas OMI measures around 13:30 local time. This means that due to the diurnal cycle of ozone it is expected that there would be more ozone in the troposphere during the OMI overpass. This could partly explain the higher tropospheric ozone amounts in the OMI retrievals. However, the photochemical production of ozone that causes the diurnal cycle takes place near the ground level and neither OMI nor IASI are sensitive there. Regarding the sensitivity of the instruments, the altitudes of maximum sensitivity of the OMI retrievals are always at the highest layer in the troposphere, while for the IASI retrievals the altitudes vary between 1 and 7 km.

Comparison of a priori ozone abundances in the troposphere (see Fig. S5) shows that the differences between the a priori values of the OMI retrievals are much smaller than between the retrieved ozone values (Fig. 9d). Moreover, as

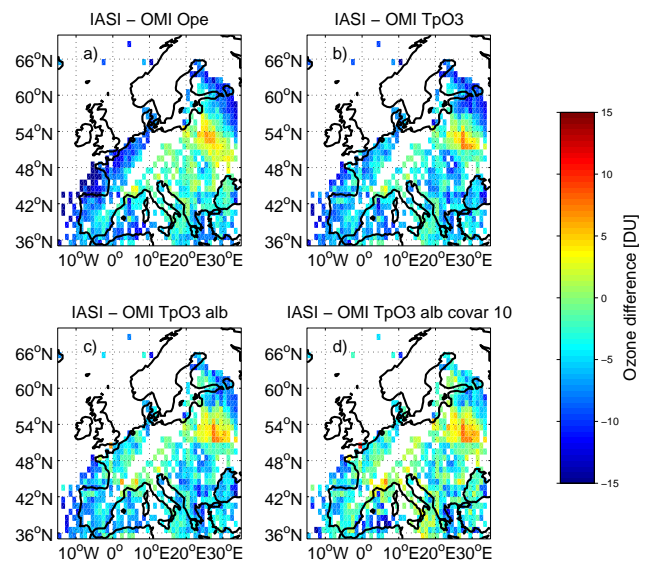


Figure 9. Difference in tropospheric ozone abundances (up to 400 hPa) between IASI and OMI on 17 July 2007. Four different versions of the OMI retrieval algorithm are used: Operational (a), TropO3 climatology and operational albedo (b), TropO3 climatology and linear albedo in UV2 (c), and TropO3 climatology, linear albedo in UV2 and climatological a priori covariance matrix (d). Daily data averaged on 1×1 grid. Statistics of the differences are given in Table 4.

the upper panels in Fig. 10 show, the IASI a priori ozone values are significantly lower than the ones used with the OMI retrievals. The IASI retrieval uses only the mid-latitude summer profile from the LLM climatology which explains the lower a priori values. This comparison indicates that the changes between the OMI retrievals in the troposphere are not governed by the a priori ozone values but that the systematic overestimation when compared with IASI retrievals can partly be caused by the higher a priori values. The lower panels in Fig. 10 show the comparisons between tropospheric ozone abundances from the OMI and IASI retrievals as scatter plots. Based on these plots, it is clear that the modified OMI retrievals (Trop_alb_covar_10) agree somewhat better

Table 6. Ground-based ozonesonde stations used in this study and the agencies authoring the data.

Stations	Latitude	Longitude	Collocated profiles	Agency
Barbados	13.2	−59.4	7	NOAA-CMDL
Beltsville	39.0	−76.7	3	Howard_U
Bratts lake	50.2	−104.7	15	MSC
Egbert	44.2	−79.8	10	MSC
Heredia	10.0	−84.1	2	U_Colorado
Holtville	32.8	−115.4	6	NASA-Ames
Huntsville	34.7	−86.6	24	UAH
Kelowna	49.9	−119.4	17	MSC
Narragansett	41.5	−71.4	21	U_RhodeIs
Paradox	43.9	−73.6	3	MEC-NY
R/V <i>R H Brown</i>	Various locations		23	NOAA-CMDL
Table Mountain	34.4	−117.7	23	NASA-JPL
Tecamec	19.3	−99.2	7	PennState_U
Trinidad Head	40.8	−124.2	17	NOAA-CMDL
Wallops	37.9	−75.5	7	NASA-WFF

with the IASI retrievals than the operational OMI. The R^2 value for the modified retrieval is 0.17 while for the operational retrieval it is almost zero (0.008). In addition, the fitted lines show that the offset of the modified retrieval is smaller and the slope is closer to one. These results indicate that the modified OMI retrieval is able to capture the tropospheric ozone patterns better than the operational retrieval.

4.2 Case study North America

The second case study was based on ozonesonde measurements over North America in August–September 2006. The ozonesonde data used in this evaluation and the agencies authoring the data are listed in Table 6. The data were downloaded from the WOUDC on 2 June 2014. We used the following collocation criteria between the sonde and satellite measurements: only ECC sondes of types 6 and Z were considered, the minimum required sonde altitude before burst was 10.0 hPa, the maximum allowed time difference between the sonde launch and satellite overpass was 3 h, and the sonde launch site was required to be situated within a OMI ground pixel. For this case study, every 5th OMI measurement and all the pixels for each measurement were taken into account. The sonde profiles were converted to partial columns, and interpolated to the pressure grid used in the OMI retrieval. The interpolated sonde profile was then convolved with the OMI averaging kernel. The resulting sonde profiles were used to calculate the differences with the retrieved and a priori OMI profiles.

Figure 11 presents the absolute and relative differences between the ozonesondes and two versions of the OMO3PR algorithm. Figure 11a and b show the relative and absolute differences for the operational OMO3PR retrieval, respectively, while Fig. 11c and d show them for the modified version (Trop_alb_covar_10). When compared with the values

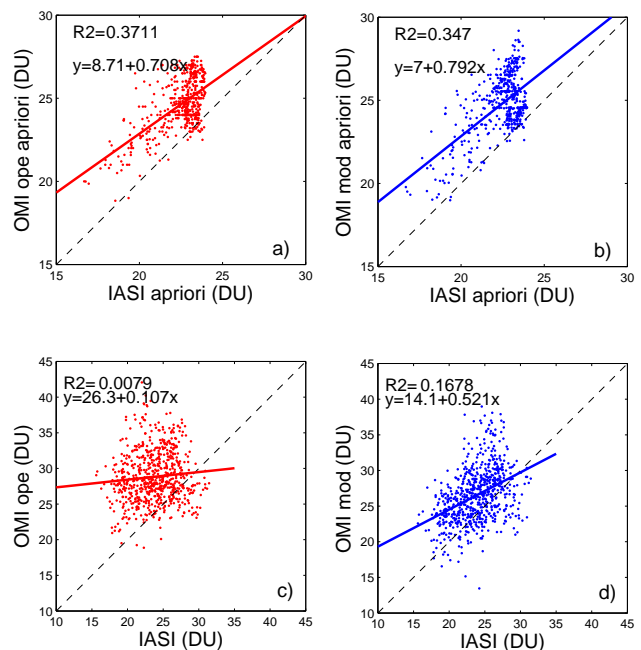


Figure 10. Comparison of tropospheric ozone abundances (up to 400 hPa) from OMI and IASI on 17 July 2007. Two different versions of the OMI retrieval algorithm are shown: operational (a, c), and modified that uses TropO3 climatology, linear albedo in UV2 and climatological a priori covariance matrix (b, d). A priori values are shown in the upper panels and retrieved values in the lower panels.

in Table 1 (ECC sondes at mid-latitude), it appears that the operational retrieval in our study agrees slightly better with ozonesondes. In Fig. 11 the lines with lighter shades of blue and red indicate the nonaveraging kernel convolved agreements with sondes. When compared with the convolved com-

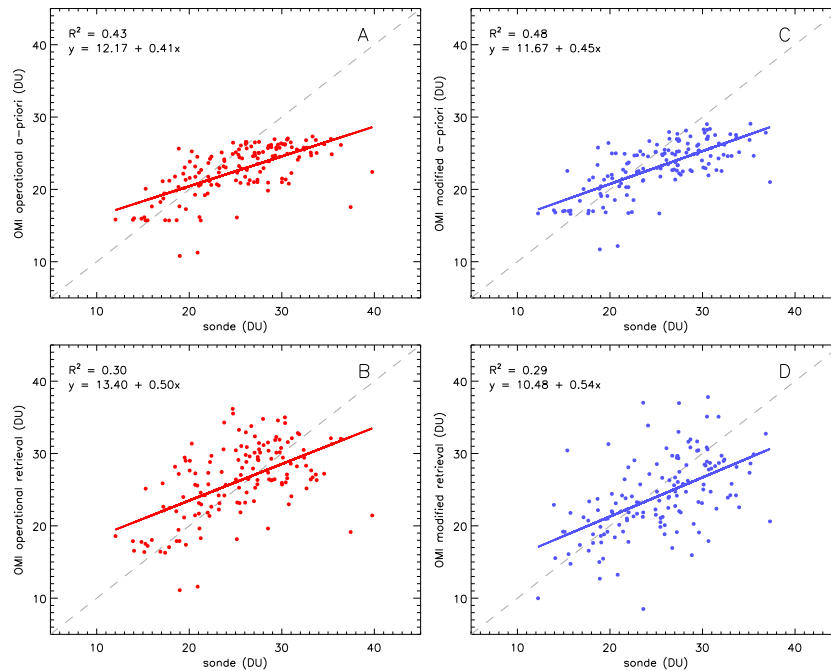


Figure 12. Comparison of tropospheric ozone abundances (up to 400 hPa) from OMI and ozonesondes over North America in August–September 2006. Two different versions of the OMI retrieval algorithm are shown: operational (**a**, **b**), and modified that uses TropO3 climatology, linear albedo in UV2 and climatological a priori covariance matrix (**c**, **d**). A priori values are shown in the upper panels and retrieved values in the lower panels.

tion < 0.3) for a better comparability with the results presented in Fig. 10. The upper panels show the comparison for the a priori data and the lower panels for the actual retrievals. As one can see from the upper plots, the a priori data in the modified (TpO3_alb_covar_10) version are slightly closer to the sonde values as the operational a priori data. The R^2 value is larger, the offset is slightly smaller and the slope is closer to one. For the retrievals (bottom plots) the situation does not change much. The difference in the offset is larger and the modified retrieval has a slightly smaller bias which was expected based on the results shown in Fig. 11. It is also worth noticing that the offset for the operational a priori is smaller than for the operational retrieval while it is the opposite for the modified retrieval. The R^2 values are almost identical and this is also in line with the previous results which indicated that the variability in the modified retrieval is larger than in the operational retrieval. The comparison with sonde data shows smaller differences between the retrieval versions than the comparison with IASI data (Fig. 10). There are several differences between the two data sets which might influence these comparisons. First of all, the IASI comparison is done for a single day with a distinct ozone pattern using gridded data whereas the sonde comparison is based on a longer period but it is limited to only 15 locations. Secondly, there are fundamental differences in the IASI and sonde data sets. Sonde data are based on in situ measurements while the IASI data set is more similar with the OMI retrievals. Thus,

not surprisingly, the evaluation results are highly dependent on the data set used in the evaluation.

We also did the scatter plot comparison using averaging kernel convoluted sonde data (see Fig. S6). This comparison produced clearly better statistics (R^2 , offset, slope) for the operational retrieval than for the modified retrieval. However, this does not mean that the modified retrieval is not as good as the operational retrieval. This just shows that the operational retrieval is not sensitive in the troposphere and it mainly uses a priori information there. The averaging kernel convolution rejects the sounding information for which the satellite measurement is not sensitive and replaces it with the a priori information. Therefore, when concentrating on altitudes where OMI is not that sensitive we are not comparing retrievals with sonde data but also with a priori data. The statistics for the modified retrieval do not change that much between these two comparisons which means that the modified retrieval is more sensitive in the troposphere than the operational retrieval.

Figure 13 presents the profiles of the averaging kernels for the operational and modified (TpO3_alb_covar_10) versions of the algorithm. It is clear that the modified algorithm has larger degrees of freedom than the operational retrieval below 20 km. Between 20 and 40 km the degrees of freedom are slightly smaller for the modified version while they are in the same range for the altitudes between 40 and 60 km. At altitudes over 60 km, the modified algorithm has clearly

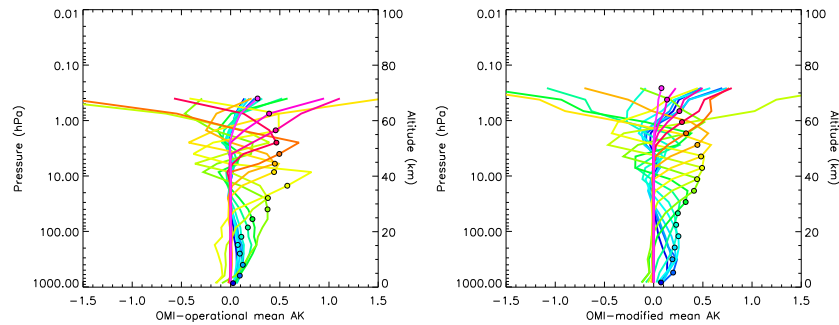


Figure 13. Averaging kernel profiles for the operational OMI retrieval (left) and the modified version with TropO3 climatology, linear albedo in UV2 and climatological a priori covariance matrix (right). Nominal altitudes for the values are indicated with small spheres. The profiles are averaged from the pixels collocated with the ozonesonde data over North America in August–September 2006.

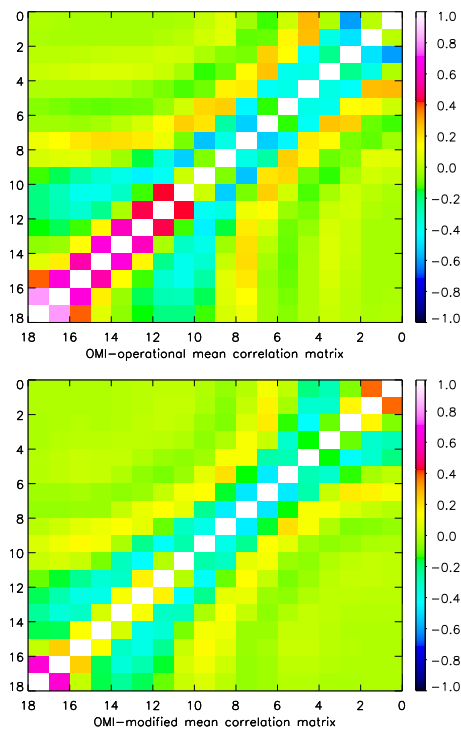


Figure 14. Correlation matrices for the operational OMI retrieval (top) and the modified version with TropO3 climatology, linear albedo in UV2 and climatological a priori covariance matrix (bottom). The matrices are averaged from the pixels collocated with the ozonesonde data over North America in August–September 2006. Axes are the layer indices, 18 being the layer closest to the surface (the corresponding pressure levels are shown in Table 3).

smaller degrees of freedom. The tropospheric layers are affected by other layers located below 20 km in both versions of the algorithm. The averaging kernels are better behaved in the modified retrieval than the operational ones because they peak at the nominal altitudes (shown as spheres) which is not the case with the operational kernels. This indicates that

the information for the tropospheric layers in the modified retrieval is mainly coming from the troposphere.

We also studied the covariance matrices of the two retrievals. Covariances are dependent on the errors, and thus it is difficult to compare covariance matrices from different retrievals. Therefore we transformed the covariance matrices to correlation matrices according to the following equation: $\text{corr}(i, j) = \text{covar}(i, j) / (\sqrt{\text{covar}(i, i)} \cdot \sqrt{\text{covar}(j, j)})$. In other words, correlation is the covariance divided by the square root of the covariance matrix diagonal. Figure 14 presents the correlation matrices for the operational and modified (TpO3_alb_covar_10) versions of the algorithm. As the figure shows, the operational version has a larger correlation in the troposphere than the modified version. This makes it harder for the operational algorithm to adjust the ozone concentration in individual layers, but the shape of the profile in the troposphere can be adjusted as a whole (as was seen in Fig. 11). In the stratosphere the correlations are similar for both retrievals except for the two highest layers which are more correlated in the modified retrieval. Figure 14 also shows that layers close to the surface (layers with indices 14–16) are anticorrelated with layers around 20 km (indices 11–13). This explains why the overestimation around 20 km was enhanced in the modified retrieval. The modified retrieval setup decreased the overestimation at the surface but it did not change the total column of ozone. Consequently, due to the anticorrelation for the ozone layers around 20 km and due to the fact that OMI has very little sensitivity for ozone around 20 km, the retrieval tends to increase the amount of ozone at these altitudes.

5 Conclusions

In order to find ways to improve the retrieval of tropospheric ozone from OMI measurements, we assessed the sensitivity of the OMO3PR algorithm to several a priori and radiative transfer assumptions. The studied assumptions were: stray light correction, surface albedo parameterization and a priori ozone climatologies. We found that stray light correction

is essential for the retrieval but it mainly affects the stratospheric layers. Surface albedo parameterization also has a significant effect on the retrieved ozone profile but mainly in the layers close to the surface. The selection of the a priori ozone profile climatology had a relatively small effect on the retrieved ozone profiles while the usage of climatological variability values in the a priori covariance matrix increased the differences significantly. Based on these sensitivity studies we modified the OMO3PR algorithm to improve the accuracy of tropospheric ozone retrievals. This was done by replacing the operational ozone climatology (LLM) with TpO3 climatology, by using climatological variability values in the a priori covariance matrix and by changing the wavelength dependency of surface albedo in the UV2 channel from a second-order polynomial to linear. Our studies showed that:

1. When compared with the IASI measurements presented by Eremenko et al. (2008) the modified version produced over 10 % smaller ozone abundances in the troposphere over Europe which reduces the systematic overestimation of the OMO3PR algorithm. Moreover, the modified version is able to capture the ozone plume in eastern Europe better than the operational retrieval.
2. When compared with ozone sonde measurements the operational retrieval performed better in the UTLS, whereas the modified version improved the retrievals in the lower troposphere and upper stratosphere.
3. The constraint on stratospheric ozone appears to have been chosen too weak, while the constraint on tropospheric ozone appears to have been chosen too strong in the operational retrieval.
4. The biases in the retrievals are not caused by the a priori information. Instead, the a priori information pushes the systematically wrong ozone profiles towards the true values.
5. The large weight of the a priori information in the troposphere in the operational retrieval damps the variability of the retrievals, and thus masks tropospheric ozone structures.
6. The modified retrieval unmasks systematic problems in the radiative transfer/instrument model and is more sensitive to tropospheric ozone variation: it is able to capture the tropospheric ozone morphology better.
7. The key to removing the systematic bias is not to adjust the weight of the a priori information but to understand the physical origin of the bias. The optimal estimation scheme is supposed to fight random instabilities resulting from the ill-posedness of the retrieval but not to fight the propagation of modelling errors.

The Supplement related to this article is available online at doi:10.5194/amt-8-671-2015-supplement.

Acknowledgements. The Dutch–Finnish built Ozone Monitoring Instrument (OMI) is part of the National Aeronautics and Space Administration (NASA) Earth Observing System (EOS) Aura satellite payload. The OMI project is managed by the Netherlands Space Office (NSO) and the Royal Netherlands Meteorological Institute (KNMI). OMI vertical ozone profile data were processed at and obtained from the NASA Goddard Earth Sciences (GES) Data and Information Services Center (DISC). We thank the World Ozone and Ultraviolet Data Center (WOUDC) for making the routine ozonesonde measurements accessible. We also thank the associate editor, T. von Clarmann and the anonymous referees whose thoughtful comments helped to improve this paper significantly.

Edited by: T. von Clarmann

References

- Acarreta, J. R., De Haan, J. F., and Stammes, P.: Cloud pressure retrieval using the O₂–O₂ absorption band at 477 nm, *J. Geophys. Res.*, 109, D05204, doi:10.1029/2003JD003915, 2004.
- Backus, G. E. and Gilbert, F.: Uniqueness in the Inversion of inaccurate Gross Earth Data, *Philos. T. R. Soc. Lond.*, 266, 123–192, 1970.
- Beer, R., Glavich, T. A., and Rider, D. M.: Tropospheric emission spectrometer for the Earth Observing System's Aura satellite, *Appl. Optics*, 40, 2356–2367, doi:10.1364/AO.40.002356, 2001.
- Bertaux, J. L., Kyrölä, E., Fussen, D., Hauchecorne, A., Dalaudier, F., Sofieva, V., Tamminen, J., Vanhellemont, F., Fanton d'Andon, O., Barrot, G., Mangin, A., Blanot, L., Lebrun, J. C., Pérot, K., Fehr, T., Saavedra, L., Leppelmeier, G. W., and Fraisse, R.: Global ozone monitoring by occultation of stars: an overview of GOMOS measurements on ENVISAT, *Atmos. Chem. Phys.*, 10, 12091–12148, doi:10.5194/acp-10-12091-2010, 2010.
- Clerbaux, C., Boynard, A., Clarisse, L., George, M., Hadji-Lazaro, J., Herbin, H., Hurtmans, D., Pommier, M., Razavi, A., Turquety, S., Wespes, C., and Coheur, P.-F.: Monitoring of atmospheric composition using the thermal infrared IASI/MetOp sounder, *Atmos. Chem. Phys.*, 9, 6041–6054, doi:10.5194/acp-9-6041-2009, 2009.
- Dobber, M. R., Dirksen, R. J., Levelt, P. F., van den Oord, G. H. J., Voors, R., Kleipool, Q., Jaross, G., Kowalewski, M., Hilsenrath, E., Leppelmeier, G., de Vries, J., Dierssen, W., and Rozemeijer, N.: Ozone Monitoring Instrument calibration, *IEEE T. Geosci. Remote*, 44, 1209–1238, 2006.
- Dufour, G., Eremenko, M., Griesfeller, A., Barret, B., LeFlochmoën, E., Clerbaux, C., Hadji-Lazaro, J., Coheur, P.-F., and Hurtmans, D.: Validation of three different scientific ozone products retrieved from IASI spectra using ozonesondes, *Atmos. Meas. Tech.*, 5, 611–630, doi:10.5194/amt-5-611-2012, 2012.
- Eremenko, M., Dufour, G., Foret, G., Keim, C., Orphal, J., Beekmann, M., Bergametti, G., and Flaud, J.-M.: Tropospheric ozone distributions over Europe during the heat wave in July 2007 observed from infrared nadir spectra recorded by IASI, *Geophys. Res. Lett.*, 35, L18805, doi:10.1029/2008GL034803, 2008.
- Forster, P. M. de F. and Shine, K. P.: Radiative forcing and temperature trends from stratospheric ozone changes, *J. Geophys. Res.*, 102, 10841–10855, doi:10.1029/96JD03510, 1997.

- Keim, C., Eremenko, M., Orphal, J., Dufour, G., Flaud, J.-M., Höpfner, M., Boynard, A., Clerbaux, C., Payan, S., Coheur, P.-F., Hurtmans, D., Claude, H., Dier, H., Johnson, B., Kelder, H., Kivi, R., Koide, T., López Bartolomé, M., Lambkin, K., Moore, D., Schmidlin, F. J., and Stübi, R.: Tropospheric ozone from IASI: comparison of different inversion algorithms and validation with ozone sondes in the northern middle latitudes, *Atmos. Chem. Phys.*, 9, 9329–9347, doi:10.5194/acp-9-9329-2009, 2009.
- Kleipool, Q. L., Dobber, M. R., de Haan, J. F., and Levelt, P. F.: Earth surface reflectance climatology from 3 years of OMI data, *J. Geophys. Res.*, 113, D18308, doi:10.1029/2008JD010290, 2008.
- Kroon, M., de Haan, J. F., Veefkind, J. P., Froidevaux, L., Wang, R., Kivi, R., and Hakkarainen, J. J.: Validation of operational ozone profiles from the Ozone Monitoring Instrument, *J. Geophys. Res.*, 116, D18305, doi:10.1029/2010JD015100, 2011.
- Levelt, P. F., Hilsenrath, E., Leppelmeier, G. W., van den Oord, G. H. J., Bhartia, P. K., Tamminen, J., de Haan, J. F., and Veefkind, J. P.: Science objectives of the Ozone Monitoring Instrument, *IEEE T. Geosci. Remote*, 44, 1199–1208, doi:10.1109/TGRS.2006.872336, 2006a.
- Levelt, P. F., van den Oord, G. H. J., Dobber, M. R., Malkki, A., Visser, H., de Vries, J., Stammes, P., Lundell, J. O. V., and Saari, H.: The Ozone Monitoring Instrument, *IEEE T. Geosci. Remote*, 44, 1093–1101, doi:10.1109/TGRS.2006.872333, 2006b.
- Liu, X., Bhartia, P. K., Chance, K., Spurr, R. J. D., and Kurosu, T. P.: Ozone profile retrievals from the Ozone Monitoring Instrument, *Atmos. Chem. Phys.*, 10, 2521–2537, doi:10.5194/acp-10-2521-2010, 2010.
- Llewellyn, E. J., Lloyd, N. D., Degenstein, D. A., Gattinger, R. L., Petelina, S. V., Bourassa, A. E., Wiensz, J. T., Ivanov, E. V., McDade, I. C., Solheim, B. H., McConnell, J. C., Haley, C. S., von Savigny, C., Sioris, C. E., McLinden, C. A., Griffioen, E., Kaminski, J., Evans, W. F. J., Puckrin, E., Strong, K., Wehrle, V., Hum, R. H., Kendall, D. J. W., Matsushita, J., Murtagh, D. P., Brohede, S., Stegman, J., Witt, G., Barnes, G., Payne, W. F., Pichè, L., Smith, K., Warshaw, G., Deslauniers, D.-L., Marchand, P., Richardson, E. H., King, R. A., Wevers, I., McCreath, W., Kyrölä, E., Oikarinen, L., Leppelmeier, G. W., Auvinen, H., Mégie, G., Hauchecorne, A., Lefèvre, F., de La Noë, J., Ricaud, P., Frisk, U., Sjöberg, F., von Scheele, F., and Nordh, L.: The OSIRIS instrument on the Odin satellite, *Can. J. Phys.*, 82, 411–422, doi:10.1139/p04-005, 2004.
- McCormick, M. P., Zawodny, J. M., Viega, R. E., Larson, J. C., and Wang, P. H.: An overview of SAGE I and II ozone measurements, *Planet. Space Sci.*, 37, 1567–1586, doi:10.1016/0032-0633(89)90146-3, 1989.
- McPeters, R. D. and Labow, G. J.: Climatology 2011: An MLS and sonde derived ozone climatology for satellite retrieval algorithms, *J. Geophys. Res.*, 117, D10303, doi:10.1029/2011JD017006, 2012.
- McPeters, R. D., Labow, G. J., and Logan, J. A.: Ozone climatological profiles for satellite retrieval algorithms, *J. Geophys. Res.*, 112, D05308, doi:10.1029/2005JD006823, 2007.
- Rodgers, C. D.: Characterization and error analysis of profiles retrieved from remote sounding measurements, *J. Geophys. Res.*, 95, 5587–5595, 1990.
- Rodgers, C. D.: *Inverse Methods for Atmospheric Sounding – Theory and Practice*, World Sci., Singapore, 2000.
- Russell III, J. M., Gordley, L. L., Park, J. H., Drayson, S. R., Hesketh, D. H., Cicerone, R. J., Tuck, A. F., Frederick, J. F., Harries, J. E., and Crutzen, P. J.: The Halogen Occultation Experiment, *J. Geophys. Res.*, 98, 10777–10797, doi:10.1029/93JD00799, 1993.
- Schoeberl, M. R., Douglass, A. R., Hilsenrath, E., Bhartia, P. K., Beer, R., Waters, J. W., Gunson, M. R., Froidevaux, L., Gille, J. C., Barnett, J. J., Levelt, P. F., and DeCola, P.: Overview of the EOS Aura Mission, *IEEE T. Geosci. Remote*, 44, 1066–1074, doi:10.1109/TGRS.2005.861950, 2006.
- Shindell, D., Faluvegi, G., Lacis, A., Hansen, J., Ruedy, R., and Aguilar, E.: Role of tropospheric ozone increases in 20th-century climate change, *J. Geophys. Res.*, 111, D08302, doi:10.1029/2005JD006348, 2006.
- Sofieva, V. F., Tamminen, J., Kyrölä, E., Mielonen, T., Veefkind, P., Hassler, B., and Bodeker, G. E.: A novel tropopause-related climatology of ozone profiles, *Atmos. Chem. Phys.*, 14, 283–299, doi:10.5194/acp-14-283-2014, 2014.
- van den Oord, G. H. J., Veefkind, J. P., Levelt, P. F., and Dobber, M. R.: Level 0 to 1 B processing and operational aspects, *IEEE T. Geosci. Remote*, 44, 1380–1397, 2006.
- Waters, J. W., Froidevaux, L., Harwood, R. S., Jarnot, R. F., Pickett, H. M., Read, W. G., Siegel, P. H., Cofield, R. E., Filipiak, M. J., Flower, D. A., Holden, J. R., Lau, G. K., Livesey, N. J., Manney, G. L., Pumphrey, H. C., Santee, M. L., Wu, D. L., Cuddy, D. T., Lay, R. R., Loo, M. S., Perun, V. S., Schwartz, M. J., Stek, P. C., Thurstans, R. P., Boyles, M. A., Chandra, K. M., Chavez, M. C., Chen, G. S., Chudasama, B. V., Dodge, R., Fuller, R. A., Girard, M. A., Jiang, J. H., Jiang, Y., Knosp, B. W., Labelle, R. C., Lam, J. C., Lee, A. K., Miller, D., Oswald, J. E., Patel, N. C., Pukala, D. M., Quintero, O., Scaff, D. M., Vansnyder, W., Tope, M. C., Wagner, P. A., and Walch, M. J.: The Earth Observing System Microwave Limb Sounder (EOS MLS) on the Aura Satellite, *IEEE T. Geosci. Remote*, 44, 1075–1092, 2006.